Measuring and understanding RF coils using a VNA

Klaus Solbach, DK3BA March 2024

RF coils play a major role in amateur radio practice, in the construction of RF circuits and in the construction of antennas. For those who did not have access to professional laboratory equipment such as LCR meters, measuring the inductance of coils was only possible for individual frequencies and via a detour, measuring the resonant frequency of a combination of the coil in question with a capacitor and recalculating using the equation for the LC resonant circuit. These days are over since inexpensive vector network analyzers appeared on the amateur market, such as the SV4401A and especially the NanoVNA with NanoVNA-Saver evaluation software /1/. This article shows how such a VNA can be used to measure coils, not just over individual frequencies, but in one sweep over a wide frequency range. The measurements with cylindrical coils and toroidal coils on iron powder- and ferrite cores show interesting frequency dependencies that are important for the use and dimensioning of coils. Further sections also examine capacitors and even resistors, which also show significant “inductor effects”.

First the calibration!

Before you can measure with a VNA, the device must be calibrated. We can use the normal calibration on the SMA sockets of the VNA, although we do not want to measure directly on the coaxial sockets, but rather a test cable is connected to the measurement object. In our case a short coax cable with ends for soldering to the coil wires. Figure 1 shows the NanoVNA-F2 used with a test cable made of RG174, pulled through a ferrite toroidal core as a precaution, and a separated inner conductor and outer conductor at the end, which are soldered to the ends of the coil winding on an iron powder toroidal core. The test cable should be separated for as short length as possible in order to deliver usable measurement results from the shortwave range to the UHF range. The separation shown in Figure 2 is approximately 6 mm long, suitable for measurements up to 100 MHz, while a 4 mm version was used for measurements up to 500 MHz.

A rough indication of the usability (not the absolute accuracy!) of this calibration is shown by measuring the reflection coefficient when connecting a low-loss cable. Figure 3 shows the magnitude of the measured reflection coefficient in dB (return loss) for a 1m long H200 Flex coaxial cable that is short-circuited at the end, a so-called “Offset Short.” For a lossless cable and with perfect calibration and error-free measurement, one would expect exactly 1 or 0 dB for all frequencies - the reflection coefficient then moves clockwise on the outer circle of the Smith Chart with increasing frequency. The cable attenuation causes the reflection coefficient to drop slightly with increasing frequency by approx. 0.3 dB at 500 MHz. This continuous drop is superimposed in the plot by a ripple in the curve, which shows a residual error after calibration. This error increases with increasing frequency but remains pleasingly low at +/- 0.2 dB at the upper

Calibration and reference plane shift

First, the standard calibration of the VNA with Open, Short and Match (OSM) is performed and saved on the SMA connector of port 1 for the S11 (reflection coefficient) measurement. This calibration applies to the “reference plane” in the SMA socket but not to the end of the measuring cable. The reference plane still has to be moved there so that an open circuit of the measuring cable also appears in the Smith Chart (S.C.) on the far right at the idle point (|S11|=1, ∢ = 0°). To do this, the “Scale” function is called up in the “Display” menu in the NanoVNA and the appropriate running time is entered under “Electrical delay”: The signals require around 33ps (pico seconds, 10-12 s) per cm of cable length divided by the shortening factor of the cable; However, twice the time must be entered as “delay” because the signals run back and forth along the cable! The optimal value can be easily adjusted with the idle measuring cable so that the phase of S11 is as close as possible to 0° for the entire frequency band. In our case, a delay of 866 ps was necessary for the 8.8 cm long cable. The reference plane shift can also be carried out in the NanoVNA-Saver PC software under the “Calibration” function if the simple delay time with a negative sign is used in “Offset Delay”. This type of reference plane shift is correct as long as the line attenuation of the measuring cable is negligible (i.e. only short cables!). If this is not the case, the calibration can be carried out directly at the end of the measuring cable: The “Open” is then the idle end and for the “Short” the inner and outer conductors are soldered to create a short circuit. The 50 Ω termination can be screwed directly onto the SMA port as a “match” without the measuring cable.

frequency end. This result suggests that measurements on coils will provide useful results. In addition to the measurement errors that can be seen in the ripple, other types of measurement errors occur. Particularly noticeable are random fluctuations, which cause the curves shown on the plot to deviate slightly from measurement run to measurement run at individual points. This also results in individual measured values for the reflection coefficient with magnitudes larger than 1 or 0 dB, which can easily be recognized as an incorrect measurement. Such result would correspond to a negative effective resistance component - a typical measurement inaccuracy of the device that can be ignored, since we of course know that the effective resistance of a coil can be small but only positive. “Acceptable” by Physics are only deviations from the outer circle to the inside! However, such errors can be reduced by averaging several measurement runs using the NanoVNA-Saver software /1/. This particularly applies to the measurement runs during calibration, as incorrect measurements during calibration are reflected in all further measurements in the calibrated state. And good practice also includes carrying out the calibration and measurements on test objects with a “warm”

VNA and constant battery voltage and in between checking the saved calibration again and again with “Open” and “Short” and repeating it if necessary.

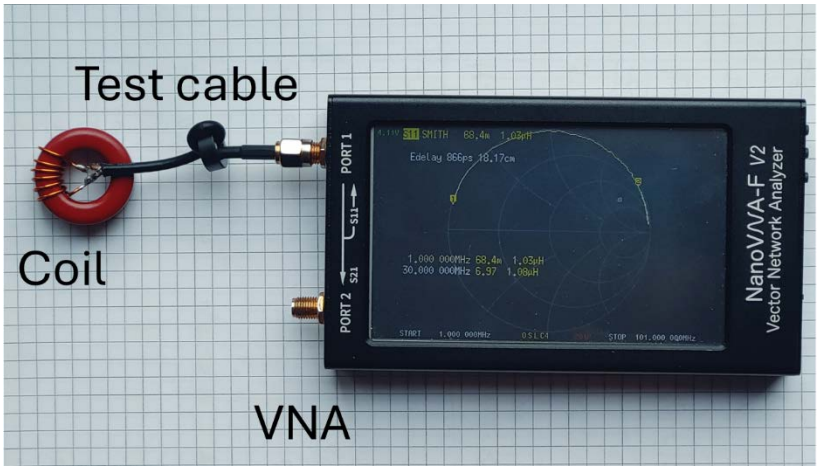

Figure 1 NanoVNA with test cable at port 1 for measuring S11 of a coil from 1 to 101 MHz.

Figure 2 Test cable with open-circuit. The inner conductor and outer conductor are separated at the end and are approx. 6 mm long.

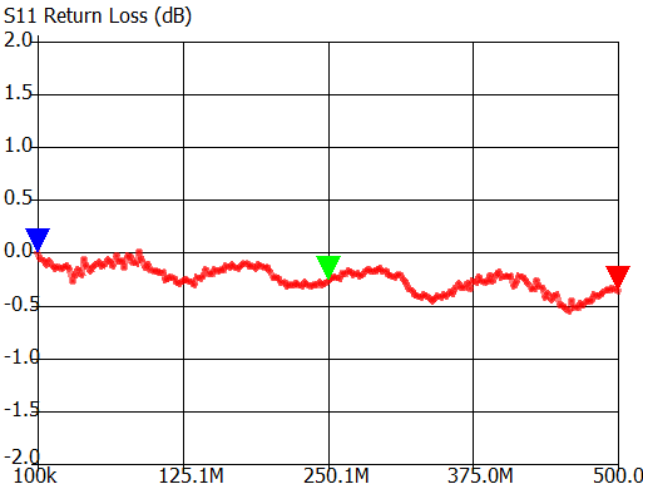

Figure 3 Return loss measured with a test cable (4mm long separation) on a 1m long cable H2000 Flex. Ripple of approximately +/- 0.2 dB at 500 MHz due to residual errors after calibration. Plot by NanoVNA-Saver PC software.

First Measurements with Calibration: Toroidal Coil

Reflection coefficient in the Smith Chart

What should the reflection coefficient (S11) of an ideal coil actually look like? "Ideal" means lossless, so the impedance of the coil should be a pure reactance *X* and this reactance should appear as pure inductance *L*, with $X = 2\pi f \cdot L$. This means that the reactance would increase exactly proportionally with the frequency *f*, and the reflection coefficient would be equal to 1 and lie on the outer circle of the S.C. where we find pure reactances. Only at an infinite frequency *X* increases to infinity and the reflection coefficient is +1 which refers to the intersection of the outer circle and the horizontal line where we find pure resistances *R*; here, both *R* and *X* are infinite. The reflection coefficient of a slightly lossy but otherwise still ideal coil should look exactly the same, just slightly within the outer circle of the S.C., so that the R-axis would be reached further inwards, with a finite resistance (e.g. in the kΩ range).

The reflection coefficient up to 500 MHz of the 6-turn coil on a T 106-2 toroidal core shown in Figure 1 was recorded in Figure 4a using the NanoVNA-Saver PC software. You can see that the measurement plot runs close to the outer edge of the S.C., but already at around 134 MHz it intersects the horizontal R-axis and then goes over into the lower part of the S.C. where capacitive impedances can be found! The separation of the measured impedance into resistance *R* and reactance *X* in Figure 4b clearly shows the behavior of a parallel resonant circuit at 134 MHz: The inductive reactance *X* increases up to the resonance frequency, where it then changes sign to become capacitive for higher frequencies. At the same time, the effective resistance *R* rises steeply from very small values up to the resonance frequency and then decays again.

Why is that?

The explanation for this behavior is the presence of "parasitic" stray capacitances between the windings of the coil, which cause the coil to even resonate: the "self-resonant frequency" (SRF), here at around 134 MHz, results from connecting the resulting total capacitance in parallel with the inductance

$$\mathrm{SRF} = 1/(2\pi \cdot \sqrt{L \cdot C}).$$

In the reflection coefficient plot shown, you can even see a small loop below the red marker, which means a further resonance mode of the coil.

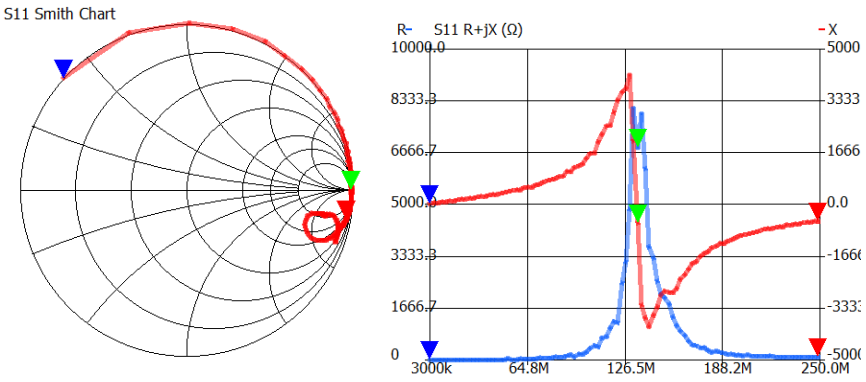

(a) (b)

Figure 4 (a) Reflection coefficient of the coil in the S.C. up to 500 MHz; Marker: blue = 3 MHz, green = 134 MHz, red = 250 MHz. (b) Division of the impedance up to 250 MHz into resistance R (blue) and reactance X (red).

The evaluation program calculates the series inductance ("Serial L") of the coil (just like the NanoVNA: in the "Marker" submenu, under "Smith Value" select the display as "R+L/C") for each frequency *f* from the corresponding reactance *X* as

$$„Serial\ L“ = X/(2\pi \cdot f)$$

In Figure 5 you can see that the inductance, like the reactance, increases steeply towards the SRF and is almost frequency-independent only at low frequencies with the flat curve. The inductance calculated in this way is also referred to as the "apparent" inductance *L**, which is related to the inductance *L* via the equation

$$L^* = L/(1 - (f/\mathrm{SRF})^2)$$

L is therefore the inductance that would be found near the frequency *f* = 0, in practice at a sufficiently low frequency where the influence of the parallel capacitance would be negligible. Common apps for calculating coil inductance and the A_L value are intended to output exactly this inductance. The equation also shows that *L** already shows 10% increase when the frequency reaches 30% of the SRF.

The resulting parallel capacitance can be calculated using the formula for the resonance frequency of an LC resonant circuit

$$C = 1/(L \cdot (2\pi \cdot f)^2)$$

In the example, *L* = 1µH, so *C* = 1.4 pF. Analogous to the apparent inductance below the SRF, there is also an apparent parallel capacitance *C**above the SRF: The evaluation software indicates around 1.1 pF for *C** at 250 MHz.

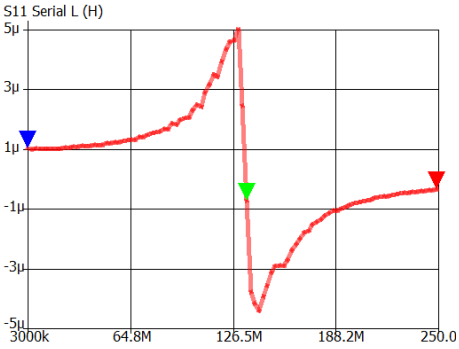

Figure 5 Calculated series inductance *L**=1.01 µH @3 MHz. *C** = 1.1pF @250MHz.

Second case: A cylinder coil

Next, a cylinder coil from an antenna project is examined, Figure 6. Twenty seven turns of 1 mm wire are wound on a 10 mm fiberglass tube over a length of approximately 46 mm. Using the OptiCoil 2.3 online calculator /2/, around 1.6 µH is calculated for the inductance with an effective resistance of around 0.8 Ω.

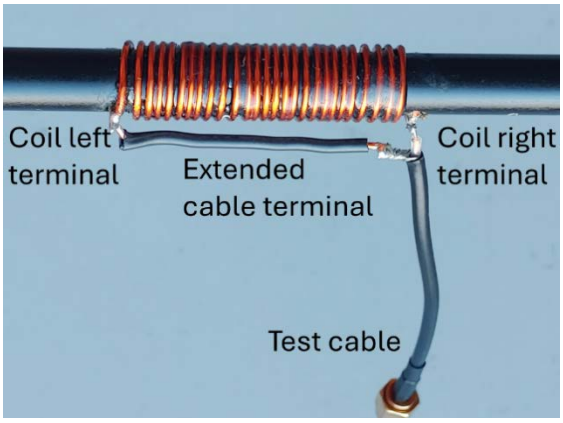

Figure 6 Coil on a GRP tube with one terminal of the test cable extended.

The measured plot of the reflection coefficient, Figure 7, is pleasingly close to the outer circle of the Smith Chart, where the purely inductive impedances can be found. There are slight outward deviations in the measurement curve, but this would correspond to a negative effective resistance component and is therefore considered a measurement error.

In the Smith Chart you can see that the reflection coefficient at 101 MHz (red marker) comes close to the intersection with the R-axis, where, as already seen with the toroidal coil, the coil's natural resonance (SRF) occurs; after expanding the frequency range of the measurement, our coil shows the SFR at around 105 MHz. Accordingly, from the calculated series inductance *L** in Figure 8 you can see an increase from around 1.6 µH at the lower frequency end up to 16 µH just below the SRF at 101 MHz. However, the test cable, with its extension of one terminal along the coil to the contact at the other end of the coil, leads to a significant increase in the parallel capacitance of the coil and thus to a corresponding reduction in the actual SFR: the natural resonance frequency of the coil without any disturbing galvanic coupling , i.e. without directly connecting the test cable, can be determined by a weakly coupling transmission measurement (of the scattering parameter S21). The two ports of the VNA couple the coil only inductively (by magnetic field) via wire loops, see Figure 9. When there is resonance, the coil transmits with maximum amplitude

from port 1 to port 2, like in a filter circuit. In Figure 10 above the first resonance, our SFR = 124 MHz (green marker), you can see even further resonances of the coil, but these do not play any role for us.

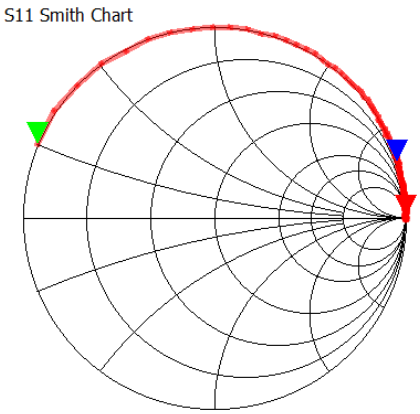

Figure 7 The reflection coefficient of the cylinder coil plotted in the Smith Chart. The markers: green = 1 MHz, blue = 30 MHz, red = 101 MHz.

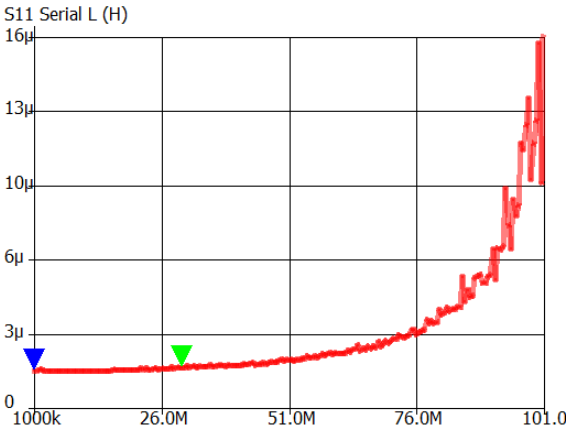

Figure 8 The “apparent inductance” (Serial L) of the cylinder coil from the measurement of the reflection coefficient. $L \approx 1.6$ µH @ 1 MHz (blue marker), L^* = 1.75 µH @30 MHz (green marker).

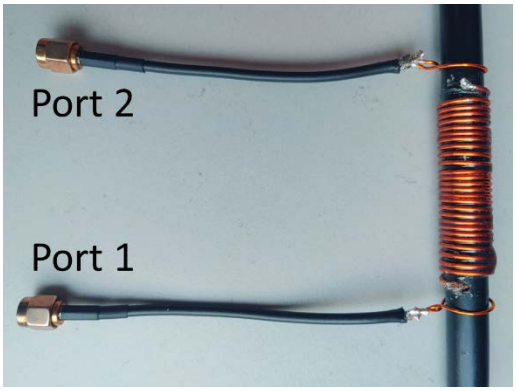

Figure 9 Cylinder coil with two coupling loops and test cables to determine the transmission coupling (S21).

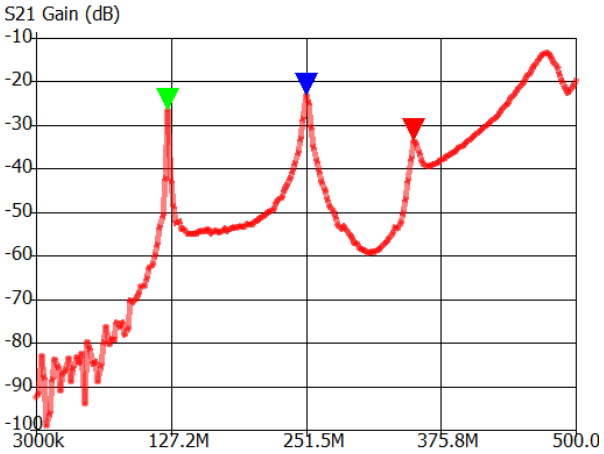

Figure 10 Transmission measurement of the solenoid coil with coupling loops. SFR = 124 MHz (green marker). Further resonances with blue and red markers.

With the SFR at 124 MHz from the S21 measurement instead of 105 MHz from the reflection coefficient measurement, the formula for *L** at 30 MHz does not result in 1.75 µH, but only 1.7 µH. However, the fact remains that in practical use in this example, as with the toroidal coil, the coils always have to be dimensioned slightly smaller than the calculation of the "classic" inductance *L* (for low frequencies) requires. In my application of the coil for inductively loading a dipole antenna for the 15 meter band, the number of turns had to be reduced by around 8% compared to the number of turns calculated with Opticoil.

Part 2

Coils on ferrite cores: A completely different behavior!

We usually find coils on ferrite in transformer and choke applications, more rarely in filter or oscillator applications. This has to do with the very special frequency dependence of the magnetic behavior of ferrites. This characteristic determines the impedance of coils, which we can measure with the VNA over a wide frequency range. As an example, we examine a coil with 3 turns on an FT 140-43 toroidal core, Figure 11.

Figure 11 Coil with 3 turns on FT 140-43 ferrite core.

At first, the plot of the reflection coefficient in the Smith Chart, Figure 12, appears to be an incorrect measurement, because apart from the first measured point at 1 MHz, all points are far away from the outer circle of the Smith Chart. This means that the coil must be subject to high losses above 1MHz due to an effective resistance. This can be clearly seen in Figure 13 from the separation of the measured impedance into resistance *R* and reactance *X*: The left plot shows the impedance from 100 kHz to 2.1 MHz and the right from 1 MHz to 101 MHz. Up to about 1 MHz you can see the behavior of a high-Q coil with about 7 µH inductance and very low resistance. In this frequency range, the ferrite material can be used well in resonance circuits. But things are different above 1 MHz: At 2.1 MHz the loss resistance rises to 20 Ω with a reactance of 105 Ω; this corresponds to a Q-factor of only about 5. In the frequency range up to 101 MHz, the resistance continues to rise to 750 Ω at 101 MHz, while the reactance levels off between 200 and 300 Ω; this looks more like a resistor with a parasitic inductance than a useful coil.

When evaluating the reactance component of the impedance, the inductance behaves unusually, see Figure 14. Up to around 2 MHz, the inductance increases to almost 8 µH, before falling sharply to less than a tenth of the inductance at low frequencies. The reason for this can be found in the permeability curves in the Amidon data sheet /3/ of the ferrite material mixture “43”.

Relative permeability

The relative permeability number μ_r indicates how much the magnetic flux in the coil core is increased by the magnetic material, and thus also how much the inductance of an air coil is increased by the core. This effect is caused by the magnetic polarization of the material - one imagines many small “elementary magnets” in the material that align themselves in sync with the magnetic field and thus support the magnetic flow. However, if the magnetic field changes direction too quickly (due to positive and negative half-waves of the high-frequency current!), the polarization can no longer follow without delay; the magnetic flux magnitude in the core decreases and shows a phase shift, increasing with the frequency of the exciting field. This behavior is described by dividing the relative permeability number into μ_r' for in-phase polarization and μ_r'' for polarization with a 90° phase shift. This wouldn't be particularly important if only the in-phase polarization, described by μ_r', can maintaine the 90° phase shift between current and voltage on an inductor, so that the coil only stores energy but does not consume any power. In contrast, the lagging polarization, described by μ_r'', supports a current in the coil that flows in phase with the voltage, as in a dissipative resistance. So μ_r' determines the inductance and μ_r'' determines an additional effective resistance of the coil. The ratio of the resistance component to the reactance corresponds to the ratio of the two permeability components μ_r''/μ_r'. The resistance component arises from a kind of frictional loss of the “elementary magnets” in the ferrite, so it represents heating of the core, while the “ohmic” resistance of the coil wire represents the heating of the conductor.

In Figure 14, the plots of the two components of the relative permeability from the data sheet are shown together with the plot of the measured inductance: The inductance drops above 3 MHz in approximately the same way as μ_r'. The increase at 2 MHz is mainly due to the parasitic capacitance, which cannot lead to resonance at higher frequencies because of the drop in inductance. The small change in reactance *X* above 3 MHz is governed by the product of frequency *f* and μ_r‘: as μ_r‘ decays about as steep as the frequency increases, the product stays nearly constant. The increase in resistance *R* up to 101 MHz and above is determined by the product of frequency *f* and μr'' and, since μ_r'' decreases less than the frequency increases, the product also increases.

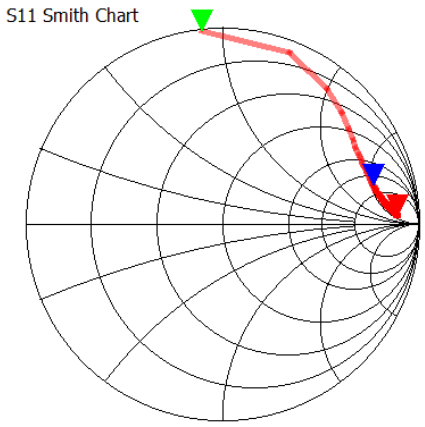

Figure 12 The reflection coefficient (S11) of the 3-turn coil on FT 140-43 in the Smith Chart from 1 to 101 MHz. Marker: green = 1 MHz, blue = 30 MHz, red = 101 MHz.

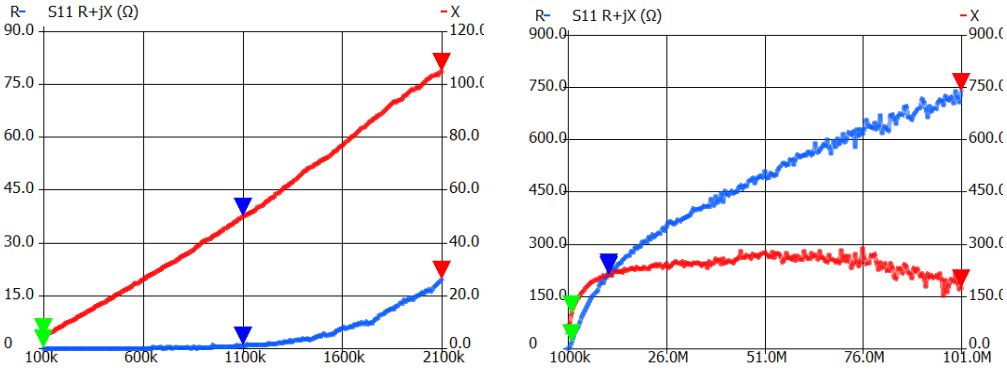

(a) (b)

Figure 13 Impedance of the coil on FT 140-43 ferrite ring, (a) from 100 kHz to 2.1 MHz, (b) from 1 MHz to 101 MHz. Reactance *X* (red) and resistance *R* (blue).

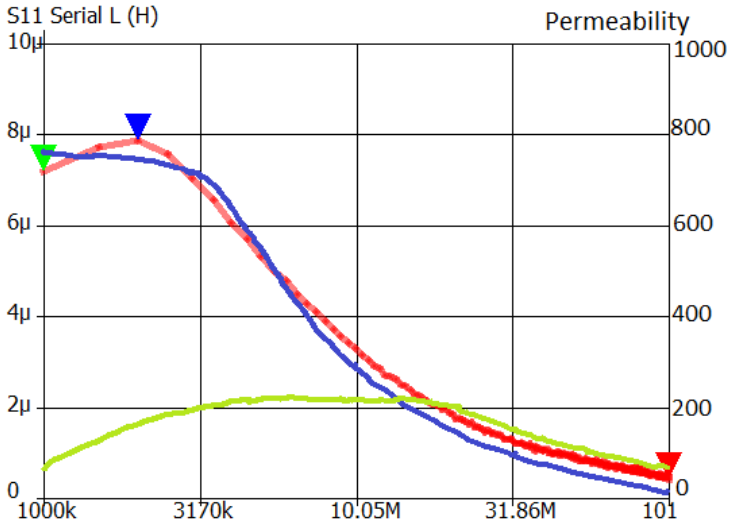

Figure 14 Inductance of the coil on FT 140-43 ferrite ring (red curve). Relative permeability μ_r' (blue) and μ_r'' (green) according to data sheet Amidon FT material "43". Frequency axis divided logarithmically.

The level of relative permeability of the material is also remarkable, from around 800 at the low frequencies to still up to 16 for μ_r' and 50 for μ_r'' at 100 MHz. This results in advantages for use in inductive transmitters/transformers. Because of the high permeability, only a few turns are necessary to generate a sufficiently high open-circuit impedance at low frequency, resonance effects are eliminated because the permeability decreases with frequency, and the close inductive coupling in the transformer still works even at high frequencies (although with slight power losses) because μ_r'' still contributes strongly to the magnetic flux where μ_r' already drops sharply.

To demonstrate this broadband characteristic in principle, a 1:1 transformer was created using a second winding in addition to the original three windings and the two windings were connected to the two test ports for measuring S11 and S21. In the Smith Chart, Figure 15, you can see the effect of the winding inductance at the lower frequency end and the effect of the stray field inductance above 12 MHz. The winding inductance is parallel to the transformer and significantly reduces the input impedance at 1 MHz with its reactance of 44 Ω. Although the unavoidable stray magnetic field of the windings is small, its inductance of around 50 nH is connected in series with the transformer and increases the impedance with increasing frequency. Nevertheless, the insertion loss (S21) is between 0.7 dB and 1.7 dB in the entire frequency range without further compensation for inductive reactive components.

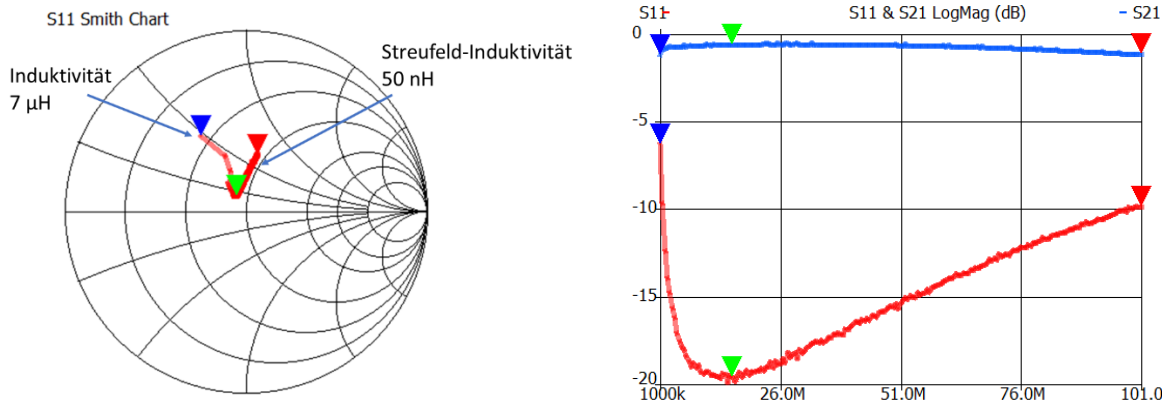

(a) (b)

Figure 15 Transformer with 2x3 turns on the FT 140-43 toroidal core. (a) Reflection coefficient in S.C., (b) S11 (red) and S21 (blue) in dB. Marker: blue = 1 MHz, green = 12 MHz, red = 101 MHz.

The second application is the implementation of broadband chokes, which act predominantly inductively at low frequencies and show high effective resistance at higher frequencies. An example from antenna technology is the “current balun” or “cable choke”.

Current Balun or Coax Choke

To suppress unwanted current on the outer conductor of a coaxial cable (also termed "common-mode" current), the cable is wound around a ferrite core. The winding forms a coil that is connected in series with the cable jacket. The higher the impedance of the coil, the less current will flow. Therefore, the coil should be operated close to the SRF, where the coil offers the highest possible impedance as a parallel resonant circuit. The ferrite core ensures that the resonance circuit is strongly damped, so that the blocking effect is broadband - for this purpose, a ferrite material must be selected that already has high values of the relative permeability μ_r'' in the frequency range to be blocked.

Our Amidon FT material "43" is well suited for the entire shortwave range up to over 100 MHz. As an example, Figure 16 shows a balun with 10 turns of RG174 cable on an FT 140-43 toroidal core. Measuring the impedance between the two ends of the cable jacket with the VNA in Figure 17 shows a range of impedance greater than 1 kΩ from 2 MHz to well over 40 MHz. At around 14 MHz the phase of S11 goes through zero, the criterion for the SRF of the coil and at this frequency you also see the largest blocking impedance of around 6 kΩ. With a lower number of turns, the SFR can be pushed higher. Since the damping permeability component μ_r'' increases, see Figure 14, the blocking bandwidth increases, but the achievable impedance also drops. For applications well above 100 MHz, a different ferrite material should be used, e.g. Amidon FT material "61".

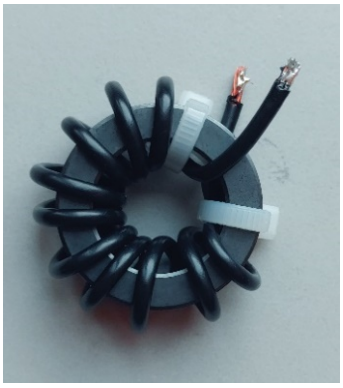

Figure 16 Current balun for the HF range made of 10 turns RG174 on FT 140-43.

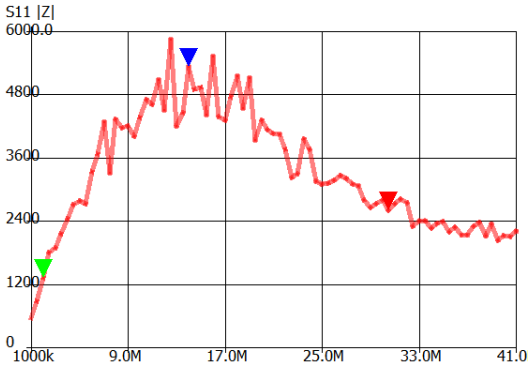

Figure 17 Magnitude of the measured impedance of the current balun. Marker: green = 2 MHz, blue = 14 MHz, red = 30 MHz. Strong excursions in the measurement plot indicate typical measurement uncertainty of the VNA at high impedances.

Another example of a ferrite-based choke is the ferrite sleeve that is slipped over a conductor; this can be a coax cable (large sleeves, used as a current balun) or much smaller, a wire in a circuit. Such a sleeve made of Ferroxcube material 3b (maximum values: $\mu_r' \approx 1000$ @

2 MHz, μ_r''≈ 600 @ 5 MHz) was examined, Figure 18: A wire through the sleeve forms a coil with an astonishingly high inductance of 1.5 µH at 100 kHz, which, however, acts like a resistance of around 60 Ω at frequencies above 25 MHz with a smaller inductive reactive component, Figure 19. This characteristic makes such a sleeve suitable as an extremely broadband barrier against the transfer of high-frequency current from, e.g., an amplifier circuit into the DC voltage supply. Smaller ferrite sleeves or “beads” are often pushed over the legs of RF transistors in order to suppress oscillation tendencies at very high frequencies.

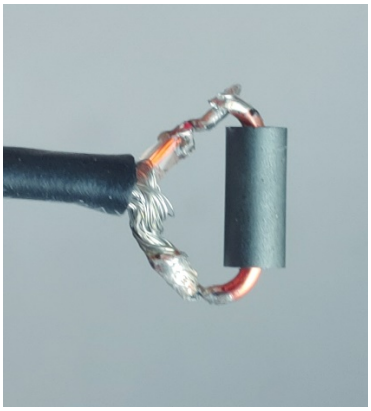

Figure 18 Ferrite sleeve Ferroxcube 3b (3.5 mm x 7.5 mm) with wire inserted through it.

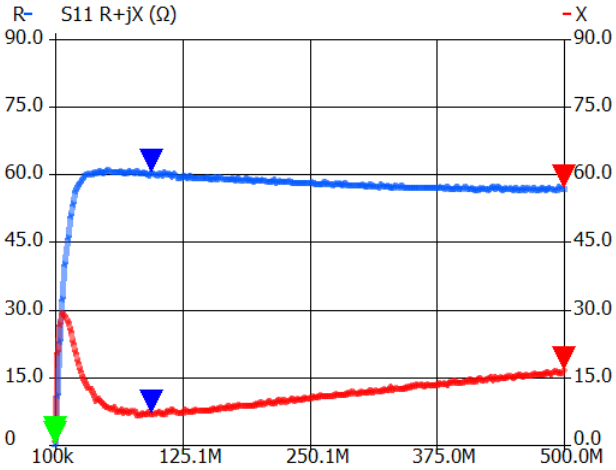

Figure 19 Impedance of the conductor loop with Ferroxcube sleeve. Blue = resistance *R*, red = reactance *X*.

Part 3

Parasitic inductance in capacitors

At first glance it seems illogical to look for inductors in capacitors. But this is what impedance testing a capacitor teaches. However, before we examine a capacitor, we should check whether the reference plane shift made during the calibration is correct: If there is a short circuit at the end of the test cable, the display must show all measuring points to be exactly on the short circuit position on the Smith Chart (left intersection of the R-axis with the SC outer circle) or the phase of S11 must be as precise as possible at 180° for the entire frequency band.

As an example, a 4.7 nF capacitor is measured. The ceramic capacitor in Figure 20 consists of an encapsulated ceramic disk, the metal coating of which is contacted in the middle on both sides with two wires about 15 mm long. To determine the S11, the test cable was soldered once directly to the end of the wires and once after shortening the wires by 9 mm - leaving about 3 mm of connecting wire to the encapsulation. The result for the shortened connecting wires in Figure 21 shows a reflection coefficient on the lower Smith Chart circle where the capacitive reactances can be found. However, the measurement plot runs through the short-circuit point at around 25.65 MHz and goes into the upper, inductive part of the SC for higher frequencies - the capacitor behaves like a coil in this frequency range. The passage through the short-circuit point makes the capacitor look like a series resonant circuit, with an inductance in series with the actual capacitor, which forms a short circuit at its resonant frequency. The magnitude of the inductance in our capacitor results from the length *l* of the conductor loop (*l* = 2 x length + 2 x width) formed by the connecting wires (wire diameter *d*). An estimate of the inductance *L* of the loop in nH of this single-layer conductor loop according to /4/ is given by the equation

$$L_{loop} = \frac{2l}{\text{cm}} \cdot \left(\ln\left(\frac{l}{d}\right) - 1{,}47 \right)$$

The longer the connection wires and the longer the loop length, the greater the inductance and the lower the resonance frequency, also called the self resonant frequency of the capacitor

$$\text{SRF} = 1/(2\pi \cdot \sqrt{L \cdot C});$$

The SRF of the capacitor with the full length of the connecting wires was correspondingly lower at 18.5 MHz. By solving the SRF formula for the inductance

$$L = 1/(C \cdot (2\pi \cdot SRF)^2)$$

The actual inductance for the wire loop can be calculated to be around 8 nH for the short version. This is consistent with the fact that the inductive reactance of the capacitor at 101 MHz (red marker) measured in Figure 21 is approximately 5.2 Ω. The capacitor behaves

“dual” to a coil over a large frequency range, with the swapping of parallel resonance to series resonance and parasitic parallel capacitance to parasitic series inductance.

Accordingly, the measurable capacity is also an “apparent” capacity *C**, which increases towards the SRF with the dual formula

$$C^* = C/(1 - (f/\mathrm{SRF})^2)$$

The evaluation software calculates the apparent capacitance from the absolute value of reactance *X* (*X* is negative for capacitance!) and the associated frequency

$$C^* = 1/(2\pi \cdot f \cdot |X|),$$

where the result can fluctuate greatly near the SRF due to division by the very small number |X|. In Figure 22, the apparent capacitance is plotted using the evaluation software: At 1 MHz we measure the capacitance for low frequencies or even direct current as around 4.5 nF, at 24 MHz *C** is already at 40 nF.

It is obvious that the SRF of capacitors depends significantly on the length of their connecting wires, given the size and capacitance of the capacitor. For some other examples, the corresponding dimensions are given in the table along with the measured SRF. One can see that for small capacitance values the SRF tends to be higher than for larger capacitance values. Because smaller capacitance values and smaller designs are often used for high RF frequencies, “wired” capacitors are still used at higher frequencies into the UHF range.

Nominal Capacitance	Type	Dimensions	Wire loop area	SRF
4,7 nF	ceram. disk	Ø 6 mm	5 x 3 mm^2	25,65 MHz
10 nF	“	Ø 8 mm	5 x 3 mm^2	17 MHz
47 nF	“	9 mm x 9 mm	8 x 3 mm^2	7 MHz
100 pF	“ 6 kV	Ø 22 mm	13 x 10 mm^2	98 MHz
56 pF	“	Ø 5 mm	5 x 3 mm^2	270 MHz
30 pF	ceram. tube	12 mm x Ø 3mm	6 x 5 mm^2	320 MHz
470 pF	FKP1 Foils	18 x 10 mm^2	14 x 3 mm^2	57 MHz
4,7 nF	SMD Multilayer	3,2 mm x 1,6 mm	----------	63 MHz
10 nF	“	“	----------	43 MHz
47 nF	“	“	----------	16 MHz

Table: Various capacitors with measured SRF.

However, the opposite case of large capacitances is problematic: Ceramic capacitors, like the one in Figure 20, are often used in RF circuits to shunt RF currents to ground, making the circuit “cold” at this point. What is necessary for this is that the impedance |Z| of the capacitor comes close to 1 Ω for all frequencies occurring at this point in the circuit, e.g. 1 – 30 MHz. The problem is that a single capacitor alone is not enough because its capacitance is

either too small for the lower frequencies or too large for the upper ones. For example, the 4.7 nF capacitor would have an impedance of less than 3 Ω from 10 - 30 MHz but would have an insufficient 35 Ω at 1 MHz. You therefore connect a capacitor with a higher capacitance in parallel, which is supposed to shunt the currents at lower frequencies. In the example a 10nF capacitor, which is still not enough to push the impedance below 3 Ω below 3 MHz, see Figure 23. This is only possible with another, larger 47 nF capacitor. However, the resulting plot of S11 in Figure 24 shows the limits of this approach: The additional capacitor reduces the impedance at 1 MHz below 3 Ω and, due to its self-resonance, pushes the impedance at 7 MHz well below 1 Ω. However, due to the inductive reactance of the 47 nF capacitor above its SRF, an additional resonance is formed (the small loop in the SC), which increases the impedance again at the medium frequencies. This problem can be avoided if five additional 10 nF capacitors are connected in parallel instead of the 47 nF capacitor.

The question remains whether capacitors without wires, i.e. SMD capacitors, do not have any parasitic inductance and do not show any natural self-resonance. Unfortunately, no, as a look at manufacturer data sheets shows. Even if an exact measurement of the SRF for a short SMD capacitor does not seem possible with the relatively coarse test cable end, three multilayer capacitors of size 1206 were measured, see Figure 25. The results for the resonance frequency are also entered in the table. Information from manufacturers of SMD capacitors of this size are not far off the mark; the measurements are apparently still “usable”. Compared to the wired capacitors, the SMD capacitors show significantly higher SRF due to a lower inductance, which should be between 1.5 nH and 2 nH with the test cable end used here.

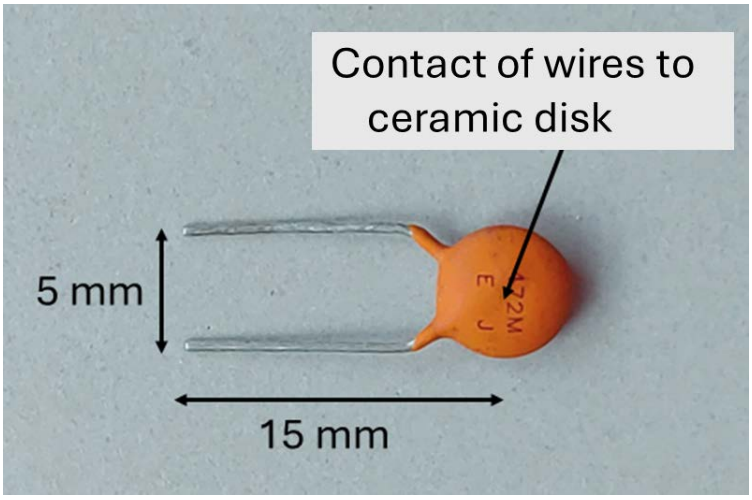

Figure 20 A 4.7nF capacitor made of encapsulated ceramic disc with long connection wires.

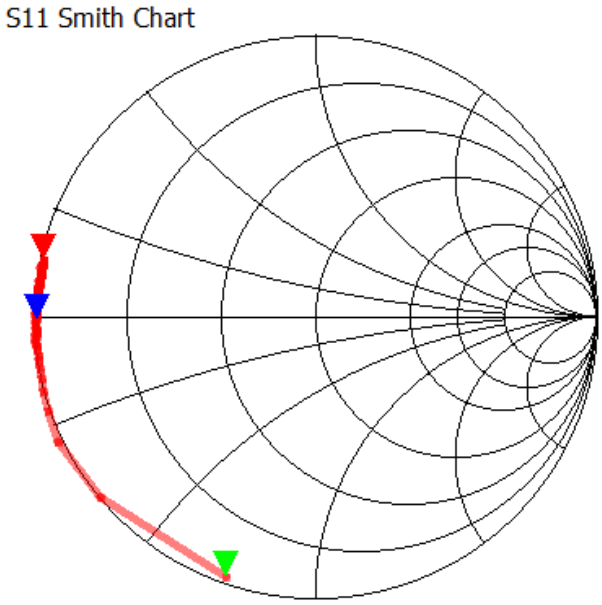

Figure 21 S11 measurement of 4.7 nF capacitor with short connection wires, marker: red=30 MHz, blue=25.65 MHz, green=1 MHz.

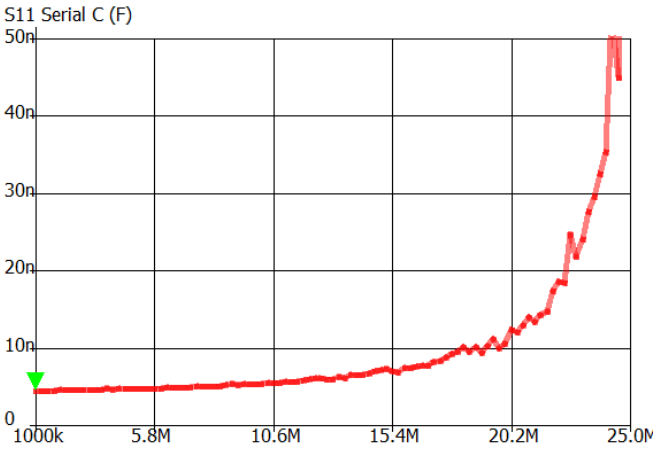

Figure 22 Apparent capacitance *C** of the 4.7 nF capacitor with short connection wires.

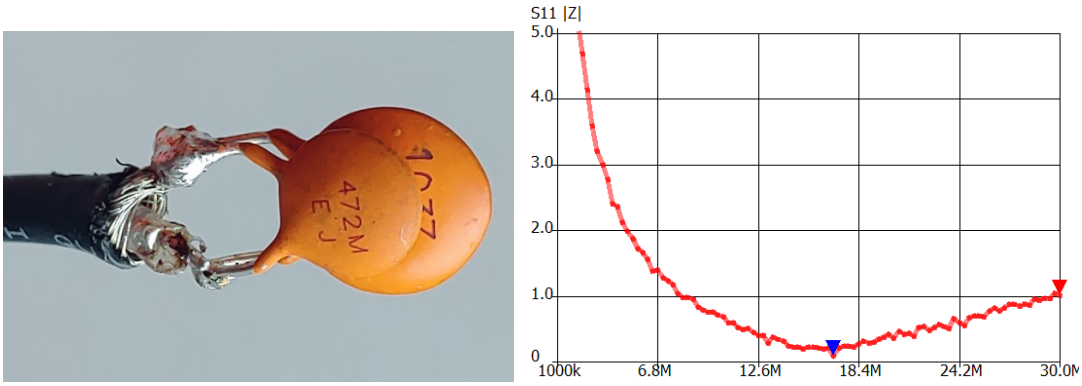

(a) (b)

Figure 23 (a) Photo of the parallel connection of 4.7 nF and 10 nF capacitors on the test cable, (b) measured reflection coefficient.

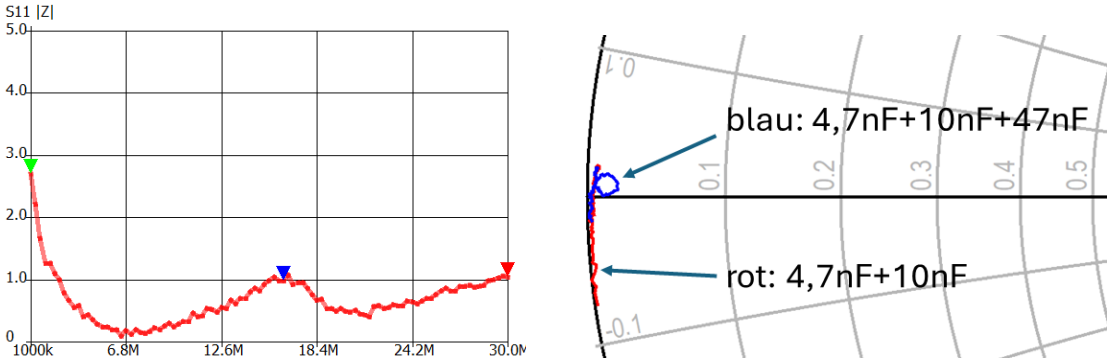

(a) (b)

Figure 24 (a) Magnitude plot of the impedance and (b) plot of the reflection coefficient in the SC for the parallel connection of 4.7 nF, 10 nF and 47 nF capacitors (in blue).

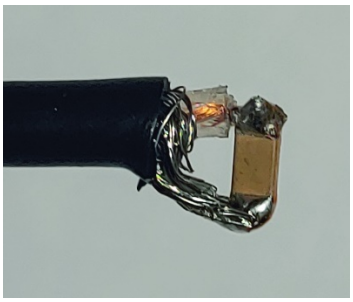

Figure 25 SMD capacitor measuring 3.2 mm x 1.6 mm on the test cable.

Equivalent circuit diagrams for coil and capacitor

As seen, the coil is plagued by its parasitic parallel capacitance, while the capacitor suffers from its parasitic series inductance. In addition, there are resistance components in both elements that cause losses: in a coil a series resistor R_V, in a capacitor a parallel conductance G_V. For coils with iron powder cores, R_V is in the order of 1/10 to 1/100 of the reactance of the coil. G_V is only 1/100 to 1/1000 of the reactance of the capacitor, which in resonant circuits can usually be neglected compared to the losses in the coil. Both loss elements cannot be determined precisely with the VNA measurement and are therefore not shown in the results, apart from coils with ferrite cores: As seen, the loss resistance can even be significantly larger than the reactance due to the special relative permeability property. In any case, the loss resistances are important parts of the coil and capacitor equivalent circuits shown in Figure 26. These equivalent circuit diagrams are valid for a large frequency range, especially well above the SRF of the coil or capacitor. I.e., except for coils with ferrite cores, the frequency dependence of the basic elements R, L, C or G, C, L can be neglected in these equivalent circuit diagrams - so circuit simulations can be easily improved by replacing coils and capacitors with their complete equivalent circuits. For coils with an iron powder core or with an air core, with a good approximation, the wire resistance of the coil winding can be taken as R_v, just taking the skin effect into account. For coils with ferrite cores, on the other hand, the inductance and the series resistance are highly dependent on the material

properties, which requires the evaluation of the permeability plot (Figure 14) in circuit simulations.

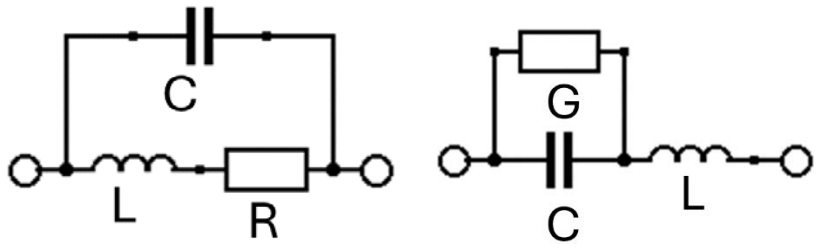

(a) (b)

Figure 26 Equivalent circuit diagrams (a) of a coil and (b) of a capacitor

Frequency dependence of resistors

If the high-frequency behavior of coils and capacitors can only be characterized by the combination of G, R, L, C elements, it makes sense to suspect that parasitic elements also have an influence on resistors. Of course, only inductance and capacitance come into question as parasitics of resistors which could determine the impedance at high frequencies.

This can be clarified by measuring the reflection coefficient or S11 of resistors. First, a thick-film resistor of a small dummy load is examined. The resistor was first measured without a heatsink in free air and showed an impedance of 49 Ω with an inductive reactance in series with approximately 44 Ω at 500 MHz, see the Smith Chart in Figure 27a. Apparently there is a series inductance of 14 nH in series with the resistor; the VSWR thus increases to 2.3 at 500 MHz. Part of this inductance is due to the widely spaced connection legs, which, together with the two conductors of the test cable, create an area of approximately 9 mm x 5 mm. By mounting the resistor on the metallic heat sink, Figure 28, the course of S11 is redirected slightly so that the mismatch is also reduced and does not reach beyond VSWR = 1.5 at 500 MHz, Figure 27b.

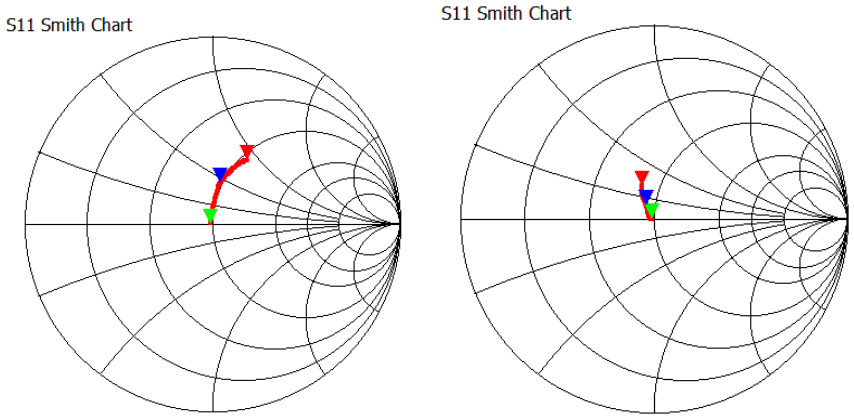

(a) (b)

Figure 27 Impedance of the dummy load in the SC. (a) Without heat sink, (b) with heat sink. Marker: green = 1 MHz, red = 500 MHz.

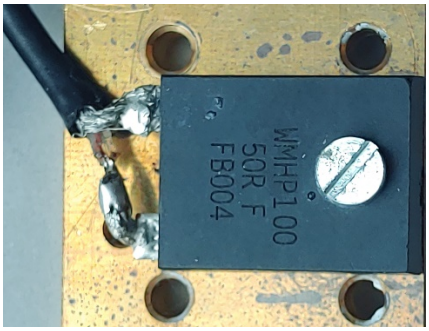

Figure 28 Power resistor 50 Ω on heat sink (dummy load)

Why does the impedance of the resistor change when it is mounted on the cooling plate? A parasitic capacitance is suspected, which could arise due to the proximity of the thick-film

conductor track in in the resistor housing to the electrically conductive surface of the heat sink. With this assumption you can model the resistance in a circuit simulator - i.e. create an equivalent circuit, as shown in Figure 29. It consists of the actual resistance R = 49 Ω and an unknown parallel capacitance C_P and a series inductance that we already know as L_S ≈ 14 nH. Simulation runs with different capacitance values then result in a more or less good fit to the measured plot of S11, but the best fit is found with C_P ≈ 3 pF. The effect of the capacitance is apparently a partial compensation for the effect of the inductance, which significantly increases the usable bandwidth of the dummy load.

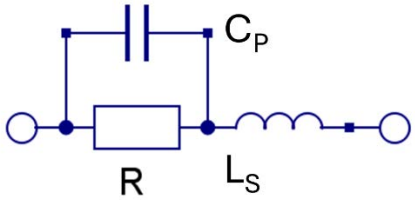

Figure 29 Equivalent circuit diagram for resistors

However, very different frequency dependencies of the impedance can be measured with low-power resistors: Metal film resistors from 25 to 1000 Ω were soldered to the test cable with the shortest possible connecting wires, Figure 30, and the S11 was recorded up to 500 MHz. It became clear that the high-resistance resistors are strongly influenced by a parallel capacitance at high frequencies, i.e. their impedance decreases with frequency, while the impedance of low-resistance resistors increases with frequency due to their series inductance. But in any case, the behavior can be well described using the equivalent circuit diagram in Figure 29 if C_P ≈ 0.5 pF is set and L_S ≈ 11 nH for each selected resistance value R. The simulation then results in the plots for the “normalized “impedance in Figure 31: The diagram shows the absolute value of impedance of a resistor divided by its resistance value for frequencies up to 500 MHz. You can read the relative increase or decrease in the impedance and compare the behavior of different resistors. The 1 kΩ impedance drops due to the parallel capacitance, the 25 Ω impedance increases due to the series inductance. In the middle range of the resistance values you can see smaller deviations, and at 100 Ω even almost complete compensation of the reactances of capacitance and inductance, so that the impedance remains at around 100 Ω up to over 500 MHz, practically ideal!

This is the reason why a 50 Ω resistor is often realized by connecting two 100 Ω resistors in parallel (even into the microwave range with much smaller SMD resistors), because then you have a 50 Ω resistor that offers perfect impedance match over a wide frequency range.

(a) (b)

Figure 30 Metal film resistors (a) wired and (b) in MELF form of size 0207 on the test cable

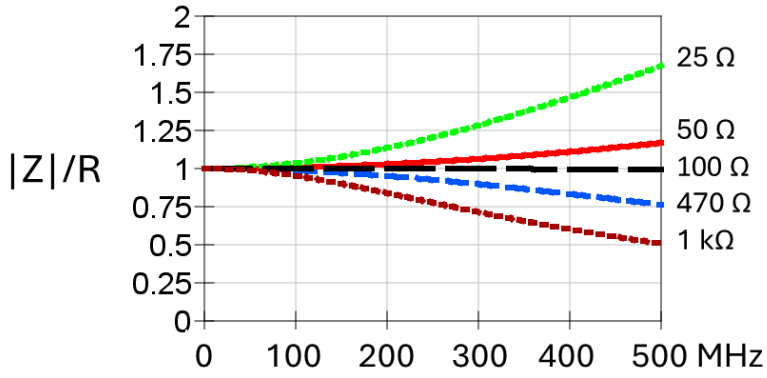

Figure 31 Simulation of the "normalized" impedance of wired metal film resistors using the equivalent circuit diagram (C_P = 0.5 pF, L_S = 14 nH). Impedance plots of MELF resistors are similar but slightly shifted to higher frequencies due to lower series inductance.

Conclusions:

In the measurements the so-called "Parasitics" of coils, capacitors and resistors show up: The parasitic capacitance in coils, parasitic inductance in capacitors and parasitic capacitance and parasitic inductance in resistors. The most important finding from this is that the inductance of a coil and the capacitance of a capacitor increase with frequency up to the self-resonance frequency SRF. This has consequences for the design of filter circuits: For example, with a Tx output LC-low pass filter, the suppression of the third harmonic is not nearly achieved if the design does not take into account that the coils and capacitors used are operated closer to the SRF in this frequency range than in lower low-pass range. Or with a load coil in a dipole antenna, the antenna is shortened too much if the coil was not dimensioned according to its "apparent" inductance, or in band-pass filter circuits the resonance frequency is always too low. For blocking capacitors, small size capacitors are to be preferred and if necessary, the wires should be kept as short as possible and, in broadband circuits, several capacitors should always be connected in parallel. When it comes to resistors in RF circuits, it is also important to use the shortest possible connection wires. At the same time, medium resistance values of around 100 Ω should be used, if necessary, connected in parallel.

References

/1/ http://www.sysjoint.com/file/Nanovna-Saver-0.3.8-by-SYSJOINT.exe

/2/ https://dxc.pi4cc.nl/tech-info/calculators/opticoil/ oder Van Roy, E, PA2EVR,“Spulenentwurf und -Optimierung komfortabel gelöst mit Opticoil V2.2“, FUNKAMATEUR 3/21, S.199 – 201

/3/ http://www.amidon.de

/4/ Meinke/Gundlach, “Taschenbuch der Hochfrequenztechnik“, Gl. (5.1), Zweite Auflage, 1962, Springer-Verlag